Photoelectron studies of the 4f and 6s subshells in atomic ytterbium

W. Agneta Svensson,* Manfred O. Krause, and Thomas A. Carlson
Oak Ridge National Laboratory, Oak Ridge, Tennessee 37831

Vojislav Radojević† and Walter R. Johnson
Department of Physics, University of Notre Dame, Notre Dame, Indiana 46556
(Received 2 August 1985)

The dynamic properties of the $4f$ subshell in atomic ytterbium were studied experimentally with the aid of synchrotron radiation and theoretically in the relativistic random-phase approximation (RRPA). Satisfactory agreement between experiment and theory was obtained for the β parameter, the $R(4f_{7/2}/4f_{5/2})$ branching ratio and the relative partial cross sections between 17.5 and 100 eV. This indicates that $4f$ photoionization is described well in the RRPA model. The properties of the $6s$ subshell were measured between 17.5 and 50 eV. In the resonance region $5p \rightarrow 5d$ the population of the three main exit channels $6s$, $4f_{7/2}$, and $4f_{5/2}$ were recorded in detail between 24 and 31 eV using the constant-ionic-state technique. For the approximately 15 resonance states similar populations of all channels were found. The $5p$ resonance structure was also calculated using a limited number of interacting channels in the multichannel quantum-defect theory.

I. INTRODUCTION

Ytterbium offers a good opportunity to study the photoionization dynamics of $4f$ electrons because due to its closed-shell structure both the experimental and the theoretical procedure can be handled conveniently. Comparison between theory and experiment has shown[1-4] that the random-phase approximation makes realistic predictions for s, p, and d electrons in closed-shell atoms in both its nonrelativistic form for light and medium atoms,[1] or in its relativistic generalization[2] (RRPA) unless the two-electron processes that give rise to photoelectron satellite lines play a major role.[5] Predictions for the f electrons have not been widely tested so far, and a comparison of theory and experiment for the $4f$ electrons of Yb is a major goal of this paper. In the only previous experimental study[6] of the $4f$ subshell, the data on the angular distribution parameter β of the $4f$ electrons in atomic Hg were seen to agree well with the RRPA predictions,[7] whereas the measured photoionization cross section σ_{4f} increased less sharply with energy than predicted by theory. However, the Hg $4f$ cross sections at the higher energies were based on an extrapolated sodium salicylate response and are subject to a correction which would improve the agreement with theory.[8]

Earlier work on ytterbium has concentrated on the two-electron transitions that occur in the region of the $5p \rightarrow 5d$ resonance. Tracy[9] measured the photoabsorption spectrum of the $5p$ subshell in ytterbium vapor between 11 and 41 eV and observed strongly autoionizing Rydberg series. Rosenberg *et al.*[10] reported electron spectra arising from electron-impact excitation of the $5p$ electrons, and Holland *et al.*[11] determined the ionic intensity ratio $I(Yb^{2+})/I(Yb^{+})$ between 20 and 35 eV. The data were interpreted in terms of autoionization and Auger decay processes. Finally, Lee *et al.*[12] reported photoelectron spectra of ytterbium at the energies of the Ne I and He I resonance lines in the first electron emission experiment on the atomic vapor.

In this paper, a study of the $4f$ subshell of atomic Yb was made over a wide energy range. For the experiment, synchrotron radiation was used to determine the important dynamic properties, σ and β, for the spin-orbit components $4f_{7/2}$ and $4f_{5/2}$ between 17.5 and 100 eV. For the theoretical predictions, the RRPA model was used to calculate σ and β from threshold to 95 eV by including the eight major channels.

In addition to the $4f$ subshell, the $6s$ subshell was studied between 17.5 and 50 eV. Measurements were made of both the relative cross section and the β parameter.

The excitation of a $5p$ electron into the empty nd ($n=5,6,7,\ldots$) and ns ($n=7,8,9,\ldots$) subshells gives rise to series of autoionization resonances, which can be observed in the available continuum channels, namely, $6s \rightarrow \epsilon l$, $4f_{7/2} \rightarrow \epsilon l$, and $4f_{5/2} \rightarrow \epsilon l$. We have measured the partial strength of these exit channels through the region that contains mainly the $5p \rightarrow 5d$ resonances and determined the β parameter for the two $4f$ channels. In doing so, we characterized the resonance structure in greater detail than is possible in a photoabsorption study. The RRPA model was also applied to the $5p \rightarrow nd$ autoionization resonances, and we report the variation in the total cross section in the region from 32 to 37 eV. We note, however, at this point that a detailed comparison of theory and experiment in the resonance region will require extension of the present theoretical and experimental work.

II. EXPERIMENTAL

The ESSR (electron spectrometry using synchrotron radiation) measurements were performed at the Tantalus

storage ring in Wisconsin with a spectrometer system that has been described previously.[4,13,14] Two electrostatic energy analyzers, mounted on a rotatable platform perpendicular to the photon beam, are used to record photoelectron spectra in suitably chosen directions. The photoelectron intensity distribution from a level i at photon energies where the dipole approximation is valid is given by

$$I_i(\phi) \propto \frac{d\sigma_i}{d\Omega} = \frac{\sigma_i}{4\pi}\left[1+\frac{\beta_i}{4}[1+3p\cos(2\phi)]\right], \quad (1)$$

where ϕ is the angle between the polarization vector of the radiation and the momentum vector of the ejected photoelectron; p is the polarization of the photons and β the angular distribution asymmetry parameter. For a given polarization p, a so-called magic angle $\phi=\phi_m$ can be chosen according to Eq. (1) such that $I_i \propto \sigma_i$. To measure the relative partial cross sections we set one of the electrostatic analyzers to ϕ_m. To measure the angular distribution parameter β, the two analyzers are set to $\phi_{\rm I}=0°(90°)$ and $\phi_{\rm II}=90°(180°)$ along the directions of the major and minor axes of the polarization ellipse. The β parameter is then obtained from the relation

$$\beta=\frac{4(R-1)}{3p(R+1)-(R-1)}, \quad (2)$$

where $R=I(0°)/I(90°)$ or $R=I(180°)/I(90°)$, and $I(\phi)$ is the electron intensity at the angles indicated.

To determine the relative partial cross sections correctly it is necessary to know the direction of the electric vector component along the major axis $E_{||}$ in the source volume, since the optical setup of the beamline in conjunction with our experimental setup can tilt $E_{||}$ out of the plane with regard to the plane of the electron beam path in the storage ring. We measured the tilt angle by recording the intensity in both analyzers and varying the angle in small steps from $-90°$ to $270°$ using a calibration photoline such as Xe $5p_{3/2}$ ($h\nu$) or Ar $3p$ ($h\nu$). The tilt angle was about $-10°$ for the toroidal monochromator (TGM) used during one period and close to $0°$ for the Seya monochromator used during another period.

The intensities $I(\phi)$ that enter the ratio R of Eq. (2) are affected by the size of the electron source volume seen at different angles ϕ and the response of the analyzers. The correction factors that needed to be applied to the observed intensity ratio R' were determined by recording the intensities of electrons which are isotropically emitted. Such electrons originate from subshells which at a given photon energy have a β parameter that equals zero. The degree of polarization was obtained from $I(0°)$ and $I(90°)$ of He $1s$ photolines for which $\beta=2$, independent of energy. The known β values for the outer subshells of the rare gases at $h\nu=21.2$ and 40.8 eV served as an additional reference allowing one to determine both the degree of polarization and the correction factors for the observed ratio.

Generally, the β parameter was obtained from Eq. (2) by determining R from the intensities measured simultaneously in two orthogonal directions with two analyzers or from the intensities measured sequentially at $0°$ and $90°$ with one analyzer. In the first case variations in photon flux and vapor pressure are eliminated, and in the second case differences in the response of the two analyzers are eliminated. As indicated above, the partial cross sections σ were obtained from data taken at the angle ϕ_m. However, the data obtained at $\phi=0°$ were also used, in conjunction with the corresponding β values, to derive σ values.

In the resonance region, data were obtained in the constant-ionic-state (CIS) mode of operation. The CIS mode previously applied to the resonances in Ga (Ref. 13) allows the rapid scanning of the resonance structure in fine steps by locking in on a photoline, which corresponds to a selected ionic state, while advancing the monochromator settings and, hence, the photon energy. Both σ and β were recorded in the CIS mode.

The bandpass of the TGM was 5 Å for one grating covering $17 \lesssim h\nu \lesssim 50$ eV and 2 Å for another grating covering $45 \lesssim h\nu \lesssim 100$ eV. The polarization varied from 94% at low energy to about 80% at 100 eV. The bandpass for the Seya monochromator was 1.6 Å and the polarization was 96% over its range up to 36 eV.

The tantalum oven[3,13,14] that was used to evaporate ytterbium of 99.99% purity was heated resistively to approximately 500°C. This temperature corresponds to about 10^{-2} Torr vapor pressure in the oven and produced a vapor density of about 10^{-4} Torr inside the source cell. During the experiment the residual gas pressure in the chamber was kept in the 10^{-8} Torr range by the use of a turbomolecular pump and a cryopump.

III. RESULTS AND DISCUSSION

A. The photoelectron spectrum

In Fig. 1 the photoelectron spectrum (PES) of atomic Yb recorded at the magic angle ($\phi_m=55.15°$) is shown displaying the relative intensities of the photolines corresponding to the final states $4f^{14}6s\ ^2S_{1/2}$, $4f^{13}6s^2F_{7/2}$, and $4f^{13}6s\ ^2F_{5/2}$ in Yb^+. The PES spectrum in Fig. 1 also exhibits satellite structure from 9.1 to 10.7 eV and around 12 eV. These satellites are due mainly to the excitation of a $4f_{7/2}$ or $4f_{5/2}$ electron into the empty $5d$ subshell and the simultaneous ionization of a $6s$ electron. All possible transitions that give rise to a singly ionized state and satellite lines[12] are listed in Table I and identified according to spectroscopic tables.[15] Many of the transitions $4f_{7/2} \rightarrow 5d$, $6s \rightarrow \epsilon l$ give rise to satellite lines that are partially hidden under the $4f_{5/2}$ photopeak; however, we estimate their contribution to the $4f_{5/2}$ photopeak to be less than 10%. Because the intensities of the satellites at 10.17 eV are low, the effects on $\sigma_{4f_{5/2}}$ and $\beta_{4f_{5/2}}$ should be small. The same statement should apply to the $6s \rightarrow nl$ and $6s \rightarrow \epsilon p$ satellites which merge with the $4f_{7/2}$ line. Extended PES spectra were recorded at two different photon energies. At $h\nu=25$ eV, additional satellite structure was observed around 14 eV binding energy. These satellites which have about half the intensity of the satellites near 12 eV presumably occur also at other excitation energies. At $h\nu=33.3$ eV, strong, sharp peaks appear at low

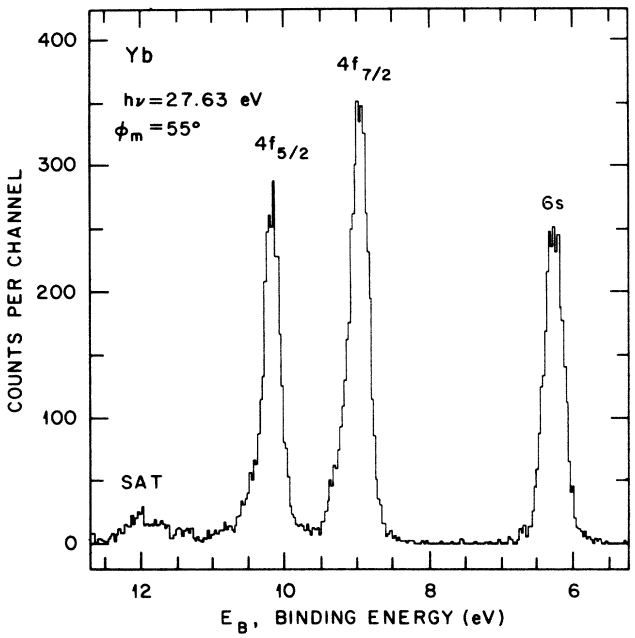

FIG. 1. Photoelectron spectrum of atomic ytterbium as recorded at the magic angle $\phi_m = 55.15°$ and a photon energy of 27.63 eV. The observed lines and the hidden satellite structure are listed in Table I.

kinetic energies. We interpret these peaks as Auger lines, since the excitation energy exceeds the $5p_{3/2}$ ionization limit. The likelihood of the occurrence of Auger-type transitions has been noted before.[9,10]

TABLE I. Ionic states of Yb associated with observed single-electron photolines and satellite lines up to 11 eV binding energy. See Fig. 1 for comparison.

Line	Ionic state[a]	E_B (eV)[a]	Remarks
1	$4f^{14}6s\,^2S_{1/2}$	6.25	6s line
2	$4f^{13}6s^2\,^2F_{7/2}$	8.91	$4f_{7/2}$ line
3	$4f^{13}6s^2\,^2F_{5/2}$	10.17	$4f_{5/2}$ line
4	$4f^{14}5d\,^2D_{3/2}$	9.10	6s satellites under $4f_{7/2}$ line
5	$4f^{14}5d\,^2D_{5/2}$	9.27	
6	$4f^{14}6p\,^2P_{1/2}$	9.61	weak 6s satellites
7	$4f^{14}6p\,^2P_{3/2}$	10.02	
4	$f^{13}(^2F_{7/2})5d\,6s\,^3D$	9.57 to 10.70	$4f_{7/2}$ satellites under $4f_{5/2}$ line
5	$f^{13}(^2F_{7/2})5d\,6s\,^1D$	9.57 to 10.70	$4f_{7/2}$ satellites in tail of $4f_{5/2}$ line
6	$f^{13}(^2F_{5/2})5d\,6s\,^3D$	9.57 to 10.70	$4f_{5/2}$ satellites
7	$f^{13}(^2F_{5/2})5d\,6s\,^1D$	9.57 to 10.70	$4f_{5/2}$ satellites

[a]According to Ref. 15. Satellite lines occurring around 12 eV are also identified in Ref. 15.

B. Theory of photoionization of the 4f subshell

The theoretical calculations of the 4f photoionization for the ytterbium atom were performed in the RRPA model[16] by including eight channels corresponding to all relativistic dipole excitations of the 4f and 6s shells, i.e.,

$$4f_{5/2} \rightarrow d_{3/2}, d_{5/2}, g_{7/2} ,$$
$$4f_{7/2} \rightarrow d_{5/2}, g_{7/2}, g_{9/2} ,$$
$$6s \rightarrow p_{1/2}, p_{3/2} .$$

The five channels obtained from dipole excitations of the 5p subshell were neglected, because some of our preliminary results gave evidence that the intrashell correlations, i.e., the correlations within the 4f shell, are dominant [there are far more electrons in the 4f shell (14), than in the 5p shell (6)], and since their inclusion will unnecessarily increase the required computer time. The main consequence of the omission of these channels resulted in a somewhat increased discrepancy between the length and velocity forms of the cross section. However, although the 6s is a very small shell, the channels from its excitations were included because the photoionization in the region close to the threshold is nearly always rather sensitive to inclusion of various types of correlations.

C. Experimental data for the 4f subshell and comparison with theory

Outside the resonance region the properties of the 4f electrons have been investigated with photons ranging from 17.5 to 100 eV. The partial photoionization cross section σ_{4f} and the angular distribution parameter β_{4f} are plotted in Fig. 2 together with the theoretical results. The data are summarized numerically in Table II. Except for the highest energies, the 4f spin-orbit components could be separated. The resulting σ component values are given in Table II by way of the branching ratio, which is also shown in Fig. 3, and the β component values are seen in Fig. 2 and Table II.

Above 45 eV, the agreement between the RRPA results and the experimental data for β is seen to be very good. Experimentally, the $\beta_{7/2}$ values are slightly higher than the $\beta_{5/2}$ values while theory predicts the same values. However, this small difference may be due to satellite lines of different kinds underlying the 4f lines. The β values below 22 eV show a similar trend as theory, but differ in magnitude. The discrepancy could be due to an inaccuracy of theory near threshold—including a shift in the threshold energies—and to a projection of the influence of the 5p resonance toward lower energies. In Hg, where no resonances occur above the 4f threshold, good accord between experiment[6] and the RRPA calculation[7] was previously found.

Satisfactory agreement between theory and experiment exists also for the σ values above about 45 eV. However, this agreement applies only to the energy dependence of the cross section since in the absence of an absolute measurement of the total photoabsorption cross section for ytterbium vapor, the experimental data needed to be normalized to theory at one point, namely $\sigma_{4f} = 3.25$ Mb at

TABLE II. Photoionization cross section for the $4f$ subshell of ytterbium, the $4f$ branching ratio, and the β parameters for the $4f_{7/2}$ and $4f_{5/2}$ components in the photon energy range $17.5 \leqq h\nu \leqq 100$ eV.

$h\nu$ (eV)	$\sigma(4f)$ (Mb)[a]	$R(4f_{7/2}/4f_{5/2})$	$\beta(4f_{7/2})$	$\beta(4f)$	$\beta(4f_{5/2})$
17.5	2.6(5)	1.9(5)	0.44(30)		0.44(30)
20.0	1.6(3)	1.6(3)	0.42(26)		0.35(45)
22.5	2.8(3)	2.2(3)	1.05(9)		0.94(8)
25.0	1.5(3)	1.65(30)	−0.5(2)		−0.0(2)
40.0	3.3(3)	1.44(10)	0.38(7)		0.37(8)
42.5	3.1(4)	1.55(17)			
45	4.2(4)	1.48(10)	0.59(8)		0.58(9)
50	4.9(4)	1.41(48)	0.60(7)		0.58(7)
55	4.7(6)	1.37(15)	0.62(13)		0.40(14)
60	4.8(6)	1.35(12)	0.56(8)		0.50(8)
65	5.3(5)	1.44(10)	0.60(9)		0.41(12)
70	5.0(7)	1.34(15)	0.44(10)		0.40(12)
75	4.6(8)	1.26(23)		0.50(12)	
80	5.6(8)	1.20(15)	0.32(10)		0.26(14)
85	5.0(9)			0.49(13)	
90	6.1(9)			0.31(11)	
100	4.5(1.1)				

[a]The value at $h\nu=40$ eV is chosen to coincide with the theoretical value of 3.25 Mb.

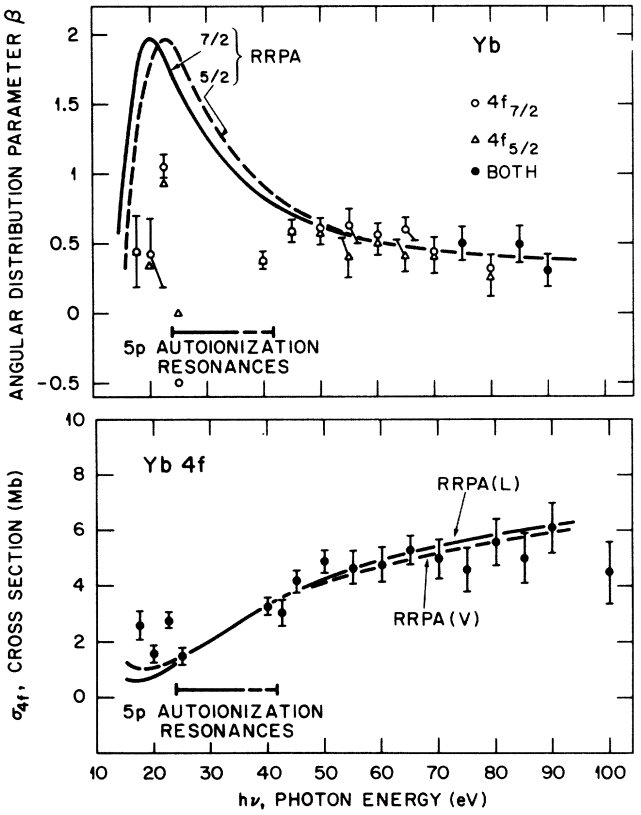

FIG. 2. Photoelectron angular distribution parameter β (upper panel) for the $4f$ electrons of Yb. Experimental data are compared with the theoretical RRPA results. Partial photoionization cross section σ of $4f$ electrons is compared in the lower panel with the theoretical velocity (RRPA-V) and length (RRPA-L) results. The experimental σ data are normalized to theory at 40 eV ($\sigma=3.25$ Mb). The behavior in the resonance region is presented in Figs. 5 and 6.

$h\nu=40$ eV. This point was chosen somewhat arbitrarily, but it is in a regime where the theoretical length and velocity results coincide and lies outside any resonance region. The experimental data tend to be lower than theory toward the higher energies, indicating a slight overestimate by theory of the centrifugal barrier acting on the $f \rightarrow \epsilon g$ channel. Near threshold, experiment and theory agree only qualitatively, as was noted for β.

The branching ratio $4f_{7/2}/4f_{5/2}$ plotted in Fig. 3 shows the same trend for theory and experiment. However, the experimental data lie below the theoretical curve above 40 eV and approach the statistical value of 1.33 at a lower photon energy than does theory. As seen from Fig. 1 and discussed in Sec. III A, satellite lines overlap with

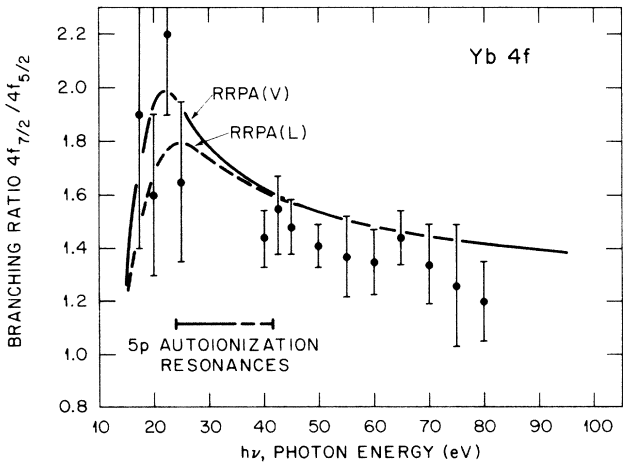

FIG. 3. Branching ratio $R(4f_{7/2}/4f_{5/2})$. Experiment (solid points) is compared with the RRPA velocity calculation (solid curve) and the length calculation (dashed curve).

the $4f$ photolines. Although the satellite contributions are small, the branching ratio of the $4f$ lines is very sensitive to even slightly unequal contributions. For example, if the $4f_{7/2},6s \rightarrow 5d,\epsilon l$ satellites under the $4f_{5/2}$ line were at least as intense as the $6s,6s \rightarrow nd,\epsilon l$ satellites under the $4f_{7/2}$ line, a lower branching ratio would result.

D. The 6s subshell

The $6s$ subshell could be studied only up to 50 eV because of its low cross section. Thus few values were obtained outside the $5p$ resonance. The data are listed in Table III. The σ values decrease slowly as a function of $h\nu$. The β values are high only at the lowest photon energy used, close to 2 at $h\nu=17.5$ eV, but are surprisingly low at the higher energies. Unless a Cooper minimum occurs near 50 eV, this behavior is at variance with previously observed trends that indicate high β values for s electrons of heavier closed-shell elements at the higher photon energies.[5,17]

TABLE III. Photoionization cross section and β parameter for the $6s$ subshell of Yb. The $\sigma(6s)$ values are normalized to $\sigma(4f)=3.25$ Mb at $h\nu=40$ eV.

$h\nu$ (eV)	$\sigma(6s)$ (Mb)	$\beta(6s)$
17.5		$\cong 2$
20.0	0.3(1)	1.4(3)
22.5	0.4(1)	1.7(3)
25.0[a]	1.0(2)	1.4(1)
40	0.13(3)	1.6(2)
45	0.17(4)	0.8(6)
50	0.13(3)	0.6(6)

[a]Within the $5p$ resonance region.

E. Theory of the 5p resonances

We also studied the $5p$ autoionization resonances in the $4f$ photoionization, within the framework of the RRPA. For this purpose we applied the multichannel quantum-defect theory[18] (MQDT) in its relativistic formulation,[19] and used the RRPA to supply the eigenchannel dynamical parameters for the MQDT analysis.

To study the resonances mentioned one needs to include in the calculations the channels from excitations of both the $5p$ and $4f$ shells. There are a total of 11 such channels. Since the $5p \rightarrow ns$ lines are not observed, we restricted our calculations to include only channels leading to $5p \rightarrow nd$ resonances, as well as the strong $j \rightarrow j+1$ and $l \rightarrow l+1$ open ($4f$) channels, and neglected the other weak ones. Thus, we took into account only five channels in our RRPA calculations, namely,

$$4f_{7/2} \rightarrow g_{9/2} ,$$

$$4f_{5/2} \rightarrow g_{7/2} ,$$

$$5p_{3/2} \rightarrow d_{5/2},d_{3/2} ,$$

$$5p_{1/2} \rightarrow d_{3/2} .$$

Although the RRPA uses theoretical Dirac-Fock values of thresholds, the MQDT analysis is performed by aligning the RRPA results with the experimental values of the $5p$ thresholds.[9] The results of our RRPA-MQDT calculations for the $5p_{3/2} \rightarrow nd$ autoionizing resonances in the energy region below the lower $5p$ threshold [$E(5p_{3/2})=31.35$ eV] are presented in Table IV. Our RRPA-MQDT results for the $5p_{1/2} \rightarrow nd$ autoioinizing resonances which are contained completely above the $5p_{3/2}$ threshold and converge to the upper ($5p_{1/2}$) threshold at 37.52 eV are presented in Fig. 4. In the last column of Table IV the predicted values of the product $(n^*)^3 f$ are given, where n^* is the effective quantum number of the line according to the Rydberg formula $\epsilon=E-1/2(n^*)^2$ (a.u.) and $f \approx \sigma_{\text{peak}}(\text{Mb})\Delta\epsilon(\text{a.u.})/4.03$ is the predicted oscillator strength of the line. If the lines converging to the ionization limit or threshold [e.g., $E(5p_{3/2})=31.35$ eV] and having the energy ϵ are of hydrogenic nature, the product $(n^*)^3 f$ is constant[20] for all members of the series, which is usually fulfilled for higher-series members.

Energies and widths of the resonances are compared with the experimental observation by Tracy[9] in Tables IV

TABLE IV. Positions, half-height widths, and peak values of the $5p_{3/2} \rightarrow nd$ autoionizing lines in the cross section of Yb predicted by the RRPA-MQDT (with five channels considered), and compared with the experimental observations (Ref. 9). Numbers in parentheses indicate powers of 10; e.g., $2.2(4)=2.2\times 10^4$.

Label (somewhat arbitrary)	Energy (eV)		n^*		σ_{peak} (Mb)	Width (eV)		$(n^*)^3 f$
	Theory	Expt.	Theory	Expt.	Theory	Theory	Expt.	
$5p_{3/2} \rightarrow 5d_{3/2}$	27.72	27.63	1.94	1.913	2.2(4)	3(−5)	0.28	0.04
$5p_{3/2} \rightarrow 6d_{3/2}$	29.85	29.99	3.01	3.16	2.1(3)	3.5(−5)	0.09	0.02
$5p_{3/2} \rightarrow 7d_{3/2}$	30.51	30.56	4.03	4.15	1.6(3)	1.5(−5)	0.06	0.01
$5p_{3/2} \rightarrow 8d_{3/2}$	30.81	30.84	5.04	5.14	1.4(3)	8.4(−6)	0.04	0.01
$5p_{3/2} \rightarrow 5d_{5/2}$	28.61	28.23	2.22	2.088	7.8(3)	5.4(−3)	0.24	4.0
$5p_{3/2} \rightarrow 6d_{5/2}$	30.07	30.21	3.26	3.463	4.7(3)	2.4(−3)	0.08	3.3
$5p_{3/2} \rightarrow 7d_{5/2}$	30.60	30.67	4.26	4.46	4.0(3)	1.2(−3)	0.05	3.2
$5p_{3/2} \rightarrow 8d_{5/2}$	30.86	30.90	5.27	5.49	3.6(3)	6(−3)	0.04	2.9

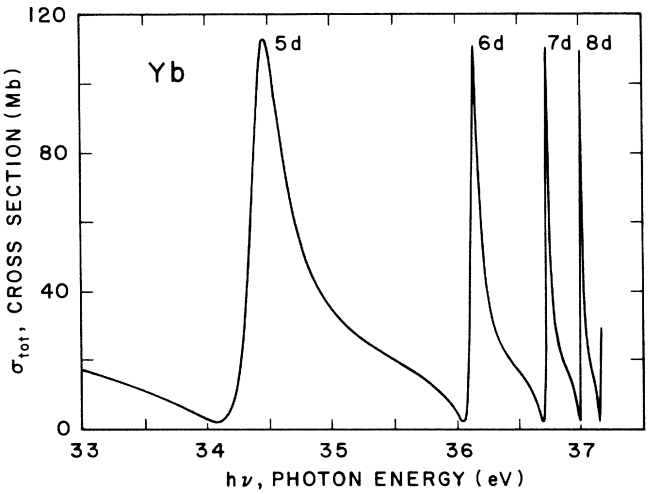

FIG. 4. Autoionizing $5p_{1/2} \rightarrow nd$ resonance profiles in the total cross section of Yb between the $5p_{3/2}$ and $5p_{1/2}$ thresholds, as calculated in the RRPA-MQDT model.

and V. There is reasonable agreement between the theoretically predicted positions of the resonance peaks, but the theoretical values of the profile widths are considerably smaller than the experimental values. The possible reasons for the discrepancy in linewidths could be either one or more of the following: the finite spectral resolution of experimental measurements, the omission of "weak" channels in our theoretical treatment, and the complete neglect of the double-electron excitations and satellites, such as the $5p^5 4f^{14} 5d^2 nl$ ($l = d,s$) states, which are very evident in the spectrum[9] of Yb. However, the RRPA cannot treat doubly excited states, and one would expect that by inclusion of these states in a theoretical treatment one would obtain better agreement with the experiment.

In the present calculation only the total oscillator strength was obtained; a breakdown of this total strength into the partial strengths that are reported in the next section would require an additional effort which would not be justified until the limitations pointed out above would have been removed.

TABLE V. Positions of peaks and widths (full width at half maximum) of $5p_{1/2} \rightarrow nd$ autoionizing resonance profiles in the cross section of Yb predicted by the RRPA + MQDT (with five channels considered) (see also Fig. 4),and comparison with the experimental observations (Ref. 9).

Label (somewhat arbitrary)	Energy (eV)		Width (eV)	
	Theory	Expt.	Theory	Expt.
$5p_{1/2} \rightarrow 5d_{3/2}$	34.47	33.29	0.36	1.4
$5p_{1/2} \rightarrow 6d_{3/2}$	36.15	36.14	0.09	0.26
$5p_{1/2} \rightarrow 7d_{3/2}$	36.73	36.73	0.04	0.16
$5p_{1/2} \rightarrow 8d_{3/2}$	37.00	37.02	0.02	<0.1

F. Experimental study of the 5p resonance

The resonance extends over the range from 24 to 37.5 eV; however, we restricted our measurements to the lower region, 24—31 eV. In Fig. 5 the relative partial strengths of the continuum channels $6s\,^2S_{1/2},\epsilon l$, $4f^{13}6s^2\,^2F_{7/2}$, ϵl, and $4f^{13}6s^2\,^2F_{5/2}$, ϵl are displayed together with the sum of these three individual spectra. The spectra were measured in the CIS mode with one of the electron analyzers set at the magic angle. In the CIS mode, data collection is computerized. Settings of the monochromator and electron analyzers were changed in 37.5-meV steps and collection time per data point was typically 35 s. A background of 3 counts per point was subtracted in each spectrum. Normalization to the photon flux and grating efficiency was done for each CIS spectrum. The labeling of Fig. 5 corresponds to the one given by Tracy.[9] The analysis of the spectra shown in Fig. 5 is summarized in Table VI and it can be seen that all three exit channels are populated for every resonance state. We note, however, a preferred and surprisingly high population of the $6s\,^2S_{1/2}$ channel for the resonance states occurring at low energies and a small population for the higher-energy resonances. Correspondingly, the $4f^{13}6s^2\,^2F$ channels show the reverse trend. Interestingly, the two major resonances, essentially peaks 7 and 11, populate the $^2F_{7/2}$ channel much stronger than the $^2F_{5/2}$ channel, namely, in the ratios 2.6 and 1.6 while the statistical ratio would be 1.33. The rather uniform population of the exit channels regardless of the res-

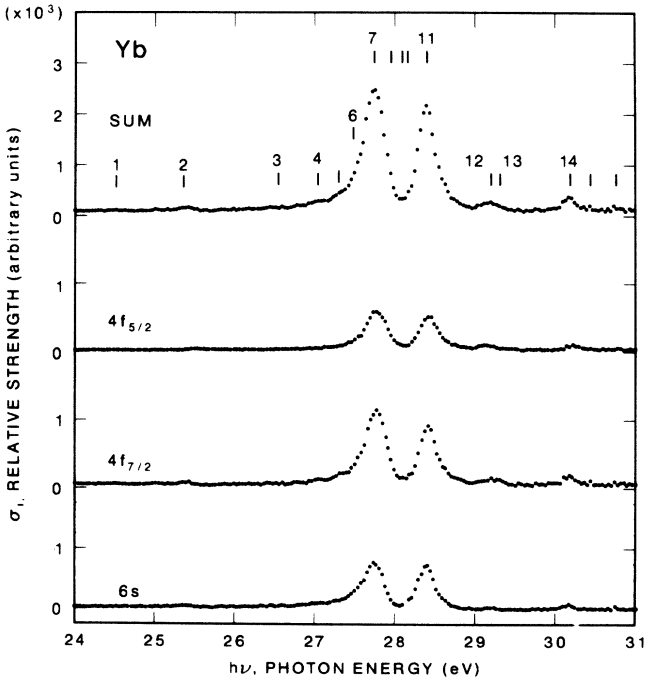

FIG. 5. Population of the three major exit channels in the $5p \rightarrow 5d$ resonance region from 24 to 31 eV and the sum of the individual contributions. The spectra were obtained in the CIS mode and are displayed in the proper proportions to one another. The peak identification is taken from Tracy's photoabsorption spectrum (Ref. 9) which is similar to the sum spectrum of this work. Peaks are generally broader than given by the monochromator bandpass of about 100 meV.

TABLE VI. Population of the resonance states (column 3) and the three major exit channels (columns 4–6) in atomic Yb as investigated by photoionization between 24 and 31 eV. Each population is normalized to 100%.

Peak No.[a]	Resonance state[a]	Sum	$6s\,^2S_{1/2}$	$4f^{13}6s^2\,^2F_{7/2}$	$4f^{13}6s^2\,^2F_{5/2}$
1	$5p^5(^2P_{3/2})$[b]	1.2	45.0	35.7	19.4
2	$5p^5(^2P_{3/2})$[b]				
3	$5p^5(^2P_{3/2})$[b]	2.5	43.4	39.4	17.1
4	$5p^5(^2P_{3/2})$[b]				
5	$5p^5(^2P_{3/2})$[b]	53.5	31.3	49.8	18.9
6	$5p^5(^2P_{3/2})$[b]				
7	$5p^5(^2P_{3/2})6s^25d[\frac{1}{2}]_1$[c]				
8	$5p^5(^2P_{3/2})$[b]				
9	$5p^5(^2P_{3/2})$[b]				
10	$5p^5(^2P_{3/2})$[b]				
11	$5p^5(^2P_{3/2})6s^25d[\frac{3}{2}]_1$[c]	36.3	38.9	37.9	23.3
12	$5p^5(^2P_{3/2})(6s\,5d^2\,^2D)J=1$	1.6	11.1	44.6	44.3
13	$5p^5(^2P_{3/2})(6s\,5d^2\,^2D)J=1$	1.7	12.6	49.9	37.5
14	$5p^5(^2P_{3/2})6s^26d[\frac{1}{2}]_1$	3.2	25.2	48.3	26.5
15	$5p^5(^2P_{3/2})6s^26d[\frac{3}{2}]_1$				
All peaks		100	29.6 ±1.5	43.7 ±2	26.7 ±2

[a]Notations according to Tracy (Ref. 9). Our energy intervals agree with those of Tracy within 15 meV.
[b]Unidentified weak lines assigned to low-lying Yb I; only the core of the configuration $5p^5(^2P_{1/2,3/2})4f^{14}5d^2(nd+(n+1)s)J=1$ is given (see Ref. 9).
[c]States labeled in jK notation.

onance state is in contrast to the observation in the $3d\rightarrow 4p$ resonance in Ga (Ref. 13) where strong preferences according to the LS state of $4p^2$ manifold were noted. This uniformity can be attributed to the fact that (a) intermediate coupling prevails in Yb imposing less restrictions on the decay paths and (b) the many two-electron excitations[9] of the outer $6s$ electrons lead to a redistribution of the transition strengths.

The sum spectrum of Fig. 5 does not correspond exactly to the photoabsorption spectrum[9] because the satellite exit channels described in Sec. III A were not included. The intensity of these additional channels amounts to 20–25% of the intensities of the single-electron channel measured at the resonance peak 7. This intensity could vary from state to state. However, according to the results given in Table VI for the main exit channels, only minor variations might be expected, so that the overall structure of the sum spectrum would be subject to only minor changes.

The presence of many two-electron excitations that couple with the $5p\rightarrow 5d$ resonances will make any calculation of this $5p$ resonance region extremely complex and difficult.

Tracy[9] reported additional, broad resonance peaks between 32 and 38 eV. We made preliminary CIS measurements of the three major exit channels in this region and observed a sum spectrum quite similar to the absorption spectrum but with much smaller intensity, relative to peaks 7 and 11, than indicated by the photoabsorption data. As the PES spectrum at $h\nu=33.3$ eV reveals, the "missing" intensity is transferred to Auger-type transitions originating in the $5p_{3/2}$ level. Adding the integrated intensity of the Auger channels to those of the three exit channels shown in Fig. 5 will indeed yield an intensity that compares well with the relative strength observed in absorption.

The angular distribution parameter β was determined over the resonance region for the spin-orbit components $4f_{7/2}$ and $4f_{5/2}$. The results are shown in Fig. 6 from 26.6 to 29.6 eV in the range that comprises the strongest resonance peaks. Data were collected in the CIS mode with one analyzer set to $\phi=0°$ and the other to $\phi=90°$. The ratios $R=I(0°)/I(90°)$ were normalized at 27.63 eV to the ratio obtained from PES spectra. The two β curves display a close resemblance throughout the resonance region except that the $f_{7/2}$ values are about 0.3 units in β

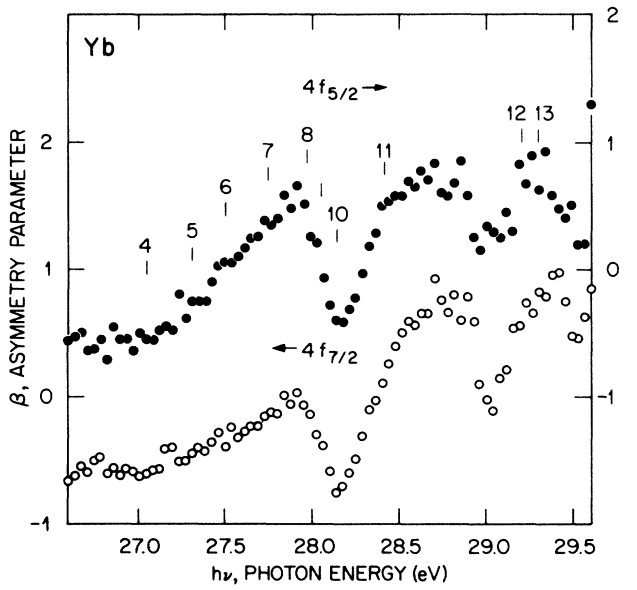

FIG. 6. Photoelectron angular distribution parameters β for the $4f$ spin-orbit components as obtained in a CIS measurement of the most intense part of the $5p \rightarrow 5d$ resonance region.

lower than the $f_{5/2}$ values. This behavior is the opposite of that noted outside the resonance range where the $f_{7/2}$ values are consistently, although only sightly, higher than the $f_{5/2}$ values. No incisive changes in β occur close to the positions of the resonance states; in fact, the β curves are rather smooth near the strong peaks 7 and 11 (compare Figs. 5 and 6). On the other hand, the β curves show a pronounced dip at the same location ($h\nu = 28.2$ eV) as the σ curves, and smaller dips at 29.1 and 29.5 eV. It appears that the weakness of the $f \rightarrow \epsilon g$ channel causes the low β value in these off-resonance positions.[21] Because the ϵg channel becomes stronger with increasing $h\nu$, the β values in the minimum should become greater with higher energies, as is in fact seen in Fig. 6, until the values shown in Fig. 2 outside the $5p$ resonances are attained.

IV. CONCLUSIONS

Photoionization of the $4f$ subshell of ytterbium has been studied experimentally by applying the ESSR technique and theoretically by using the RRPA model. Ytterbium is one of the few elements in which the properties of f electrons can be probed in a free atom with a closed-shell structure. The comparison between theory and experiment for the partial cross sections and the β parameters demonstrates that the RRPA calculations give reliable results for the dynamic parameters of the $4f$ electrons outside the resonance regions. At this time, the conclusions drawn from the σ results are based on the energy dependence of σ and are, hence, not as definitive as if they were based on absolute values of σ. Absolute experimental values of the total or partial photoionization cross sections still remain to be determined.

The strong $5p \rightarrow 5d$ autoionization resonance was also investigated, both theoretically and experimentally. Theoretical resonance energies were found to agree satisfactorily with our experimental energy values and those by Tracy, but the calculated widths were found to be narrower than the experimental widths observed in photoabsorption measurements. An improvement could, in principle, be achieved if more channels were included in the calculation, but in practice this would lead to extremely complex calculations. The exit channels for the autoionization resonance states were identified and the population of the three major channels involving the $4f_{7/2}$, $4f_{5/2}$, and $6s$ electrons were measured. No drastic variation in the population of the exit channels was observed for the different resonance states. The β parameters for the $4f$ spin-orbit components were found to display a similar behavior across the strong resonance states. Interestingly, no strong variation in the β values was observed at the positions of the strong resonances. In the resonance region above the $5p_{3/2}$ threshold the occurrence of Auger decay channels was verified, but a detailed study of this region is yet to be undertaken.

After completion of the manuscript we learned of a very recent RRPA calculation which considers 21 channels for the excitation of the $6s$, $4f$, $5p$, $5s$, and $4d$ subshells.[22] These new results are similar to ours, but yield cross-section values that are on the average 30% higher than ours.

ACKNOWLEDGMENTS

Research sponsored in part by the Division of Chemical Physics, Office of Basic Energy Sciences, U.S. Department of Energy under Contract No. DE-AC05-84OR21400 with the Martin-Marietta Energy Systems, Inc., and in part by National Science Foundation (NSF) Grant No. PHY-83-08136. The experiments were carried out at the Synchrotron Radiation Center, Stoughton, WI which is supported by NSF Grant No. DMR-83-13523.

*Present address: Royal Institute of Technology (FYSIK I), S-100 44 Stockholm, Sweden.

†Permanent address: Theoretical Physics Department, Boris Kidrič Institute, Vinča, P. O. Box 522, 11001 Beograd, Yugoslavia.

[1] M. Ya. Amusia and N. A. Cherepkov, Case Stud. At. Phys. 5, 47 (1975); G. Wendin, in *Photoionization and Other Probes of Many-Electron Interactions*, edited by F. J. Wuilleumier (Plenum, New York, 1976), pp. 61–82; M. Ya. Amusia, N. A. Cherepkov, Dj. Zivanović, and V. Radojević, Phys. Rev. A **13**, 1466 (1976); M. Ya. Amusia, N. A. Cherepkov, I. Pavlin, V. Radojević, and Dj. Zivanović, J. Phys. B **10**, 1413 (1977).

[2] W. R. Johnson and K. T. Cheng, Phys. Rev. A **20**, 978 (1979); W. R. Johnson, V. Radojević, P. Deshmukh, and K. T.

Cheng, *ibid.* **25**, 337 (1982); V. Radojević and W. R. Johnson, J. Phys. B **16**, 177 (1983).

[3]M. O. Krause, W. A. Svensson, T. A. Carlson, G. Leroi, D. E. Ederer, D. M. P. Holland, and A. C. Parr, J. Phys. B **18**, 4069 (1985).

[4]M. O. Krause, T. A. Carlson, and P. R. Woodruff, Phys. Rev. A **24**, 1374 (1981).

[5]A. Fahlman, M. O. Krause, T. A. Carlson, and A. Svensson, Phys. Rev. A **30**, 812 (1984).

[6]P. H. Kobrin, P. A. Heimann, H. G. Kerkhoff, D. W. Lindle, C. M. Truesdale, T. A. Ferrett, U. Becker, and D. A. Shirley, Phys. Rev. A **27**, 3031 (1983).

[7]W. R. Johnson and V. Radojević, Phys. Lett. **92A**, 75 (1982).

[8]According to a most recent measurement of the response curve [D. A. Shirley (private communication)].

[9]D. H. Tracy, Proc. R. Soc. London, Ser. A **357**, 485 (1977).

[10]R. A. Rosenberg, S.-T. Lee, and D. A. Shirley, Phys. Rev. A **21**, 132 (1980).

[11]D. M. P. Holland, K. Codling, and R. N. Chamberlain, J. Phys. B **14**, 839 (1981).

[12]S.-T. Lee, S. Süzer, E. Matthias, R. A. Rosenberg, and D. A. Shirley, J. Chem. Phys. **66**, 1496 (1977).

[13]M. O. Krause, F. Cerrina, and A. F. Fahlman, Phys. Rev. Lett. **50**, 1118 (1983).

[14]M. O. Krause, T. A. Carlson, and A. Fahlman, Phys. Rev. A **30**, 1316 (1984).

[15]W. C. Martin and L. Hagen, *Atomic Energy Levels - The Rare Earth Elements,* Natl. Bur. Stand. (U.S.) Natl. Stand. Ref. Data Ser. No. 60 (National Bureau of Standards, Gaithersburg, Maryland, 1978).

[16]W. R. Johnson and C. D. Lin, Phys. Rev. A **20**, 964 (1979).

[17]S. T. Manson and A. F. Starace, Rev. Mod. Phys. **54**, 389 (1982); A. Niehaus and M. W. Ruf, Z. Phys. **252**, 84 (1972).

[18]M. J. Seaton, Proc. Phys. Soc. London **88**, 801 (1966); U. Fano, Phys. Rev. A **2**, 353 (1970).

[19]C. M. Lee and W. R. Johnson, Phys. Rev. A **10**, 1598 (1980).

[20]U. Fano and J. Cooper, Rev. Mod. Phys. **40**, 441 (1968).

[21]G. Wendin (private communication).

[22]P. Deshmukh and S. T. Manson (private communication).